

Maximizing the electric field strength in the foci of high numerical aperture optics

Markus Sondermann,* Norbert Lindlein, and Gerd Leuchs
*Institute of Optics, Information and Photonics,
Max Planck Research Group,
University of Erlangen-Nuremberg,
91058 Erlangen, Germany*

Several applications require spatial distributions of the incident electric field that maximize the electric field at a focal point for a given input power. The field distributions are derived for various optical systems in a direct way based on fundamental physical properties. The results may prove useful for a wide range of applications, e.g., microscopy, scattering experiments or excitation of single atoms. For commonly used distributions - fundamental Gaussian modes and doughnut modes - we give the upper bounds of the achievable field amplitudes.

I. INTRODUCTION

Recently, there has been increased interest in the interaction of single matter systems like atoms, molecules or ions with weak light beams or single photons in free space. The topical spread covers scattering by single two-level systems [1, 2, 3, 4, 5] as well as the absorption of single photons by single atoms [6, 7, 8]. Also other applications relying on high numerical aperture (NA) optics have raised increasing attention, involving parabolic mirrors [9, 10] as well as lenses [11].

It is common to all these applications that they require the smallest possible focal volume or – in other words – that the power incident onto the focusing optics is transformed in such a way that the electric energy density in the focus is maximized. Thus, one wants to maximize the amplitude of the electric field in the focus. Although it is well known since quite some time that the optimum performance is achieved by electric dipole radiation [12, 13, 14] and also some newer publications hint in this direction [15, 16], this recipe is followed only in few papers in a consequent manner [5, 6, 7]. There are also publications in which some sort of ‘optimization procedure’ is followed: In Ref. [4] the beam width of a circularly polarized fundamental Gaussian is varied in order to maximize the strength of the circularly polarized field component in the focus of an aspheric lens. The authors of Ref. [10] follow a similar procedure in varying the beam waist of a radially polarized doughnut beam during minimization of the focal volume in the case of a parabolic mirror. In both cases, the optimization procedure is equivalent to maximizing the overlap of the incident radiation with dipole radiation. In the former case [4] the Gaussian fundamental mode is matched towards the distribution that creates the field of a circular dipole after refraction by the focusing lens. In the latter case [10] the doughnut mode is adapted such that it best overlaps with the field of a linear dipole that has its axis parallel to the optical axis of the parabolic mirror. Finally, in a recent paper the field distribution that maximizes the focal field component parallel to the optical axis of a high NA lens is directly calculated by a variational method [11]. However, with the exemption of Ref. [10] no direct and explicit relation between the found

optimal radiation modes at the input and a dipole radiation pattern is given in these publications.

Based on earlier results obtained by others [12, 13] we follow a different approach in what follows here. Knowing that it is only electric dipole radiation that contributes to the focal electric field (see, e.g., Refs. [12, 16]), we calculate the distribution of the field incident onto the focusing device that gives the desired dipole radiation pattern after reflection/refraction by the focusing optics, as it was done for a parabolic mirror and linear dipole radiation in Ref. [6]. This approach is on the one hand the most direct one. On the other hand, it is conceptually simple in comparison to other methods. Besides temporal/spectral issues not treated here, this ansatz is the same as the time reversal argument given in Refs. [6, 7] (see also, e.g., Ref. [17] for time reversal focusing of microwaves and Ref. [18] for acoustic waves).

Some of the results obtained here can in parts also be found in other publications [13, 19, 20, 21]. However, a comprehensive study that covers all practically relevant cases is still lacking. Therefore, this paper is intended to deliver a recipe for maximizing the electric field in focusing applications, in particular the excitation of single atoms as envisaged in Refs. [3, 4, 5, 7]. In the next section, we will emphasize the importance of a large solid angle of illumination. In Secs. III and IV the optimal intensity and polarization distributions will be derived for the cases of illumination by means of a parabolic mirror, a lens fulfilling the sine condition and an ideal thin lens. Since the experimental realization of these distributions may turn out to be rather involved, the overlap of ‘standard’ radiation modes with the ideal ones is treated in Sec. V.

Unlike in many other publications where the field in the focal region is treated, the discussion will be restricted to the electric field in the very focal point itself. For the main applications in mind here – scattering by single atoms or absorption of single photons – this constitutes a well justified restriction, since it is only the field at the location of the atom that matters (see also Ref. [4, 5, 16]). Furthermore, this restriction leads to several simple analytical results.

II. INFLUENCE OF THE SOLID ANGLE

Before starting with the calculations, we make some notes on the terminology used in this paper. For the quantum-optical

*Electronic address: markus.sondermann@physik.uni-erlangen.de

applications mentioned above, the field parallel to an atomic dipole has to be maximized. In these cases, the 'dipole axis' is given by the quantization axis of the scenario at hand. In a classical sense, the term 'dipole axis' designates the direction from which the polar angle ϑ is measured that parameterizes the angular dipole radiation patterns (see also Fig. 1). However, one may also think of applications in which no particular emitter or source is present at the focus but one wants to maximize the electric field vector that points into a certain direction. This field vector can be thought of as being parallel to some imagined dipole moment. Thus, we will adopt the terminology of Ref. [5] and often speak of 'virtual dipoles', i.e., dipoles that *would* produce a certain kind of radiation pattern but are not present in reality.

The term 'solid angle' usually designates the integral over the covered polar angle and the covered azimuthal angle. Here, we use this term in a slightly different context. It designates the covered solid angle weighted by a certain dipole emission pattern: $\Delta\Omega = \int D(\vartheta) \sin\vartheta d\vartheta d\varphi$, with $D_\pi(\vartheta) = \sin^2\vartheta$ for a linear dipole or $D_{\sigma_\pm}(\vartheta) = (1 + \cos^2\vartheta)/2$ for a circular dipole [22], respectively. Thus, the maximum achievable, weighted solid angle is $\Delta\Omega_{\max} = 8\pi/3$ instead of 4π in the usual sense.

We now derive an analytic expression that highlights the influence of the covered solid angle. The electro-magnetic field can be decomposed into its different multipole components. This has been exploited in Ref. [20] to calculate the field in the focal region for a given input field. However, since we are only interested in the field at the focus, which we take to coincide with the origin of our coordinate system, we only need to take care of the dipole components. Furthermore, it has already been pointed out in Ref. [19] that each kind of dipole radiation creates predominantly its respective state of polarization at the focus/origin. This is exactly true for dipoles oriented along the optical axis of the focusing system. Therefore, it is obvious that one only needs to create the radiation pattern of a single kind of dipole for most practical cases.

In order to calculate the (time independent) field in the focus, we use the Debye-integral in the form given in Ref. [23]:

$$\mathbf{E}(0) = -i \frac{f}{\lambda} \int \mathbf{E}_f(\vartheta, \varphi) \sin\vartheta d\vartheta d\varphi \quad , \quad (1)$$

where $\mathbf{E}_f(\vartheta, \varphi)$ is the field on the focal sphere for a focal length f , φ is the azimuthal angle and λ the wavelength of the light to be focused. Furthermore, a term $\exp(i\mathbf{kr})$ has already been dropped since we treat only the case $\mathbf{r} = 0$.

If only a single kind of dipole radiation is incident onto the focus, the field on the focal sphere can be written as $\mathbf{E}_f = \psi_d \mathbf{p}_d$, where ψ_d is a proportionality factor and \mathbf{p}_d is the polarization vector of dipole radiation in the far field with $d = \pi, \sigma_\pm$ for a linear or circular dipole, respectively. The polarization vectors in spherical coordinates are given by [24]

$$\mathbf{p}_\pi = -\sin\vartheta \mathbf{e}_\vartheta \quad (2)$$

and

$$\mathbf{p}_{\sigma_\pm} = \frac{1}{\sqrt{2}} (\cos\vartheta [\cos\varphi \pm i \sin\varphi] \mathbf{e}_\vartheta + [\pm i \cos\varphi - \sin\varphi] \mathbf{e}_\varphi) \quad (3)$$

with $\mathbf{e}_{\vartheta, \varphi}$ being the polar and azimuthal unit vectors.

Next, we require that independent of the covered solid angle the power P incident onto the focus is a constant (this would correspond to the case of, e.g., a single photon that is focussed with lenses of different numerical aperture but always covers the whole lens cross section). The total power radiated through the surface of the focal sphere can be written as

$$P = \frac{1}{2} \epsilon_0 c f^2 \int_{\varphi_1}^{\varphi_2} \int_{\vartheta_1}^{\vartheta_2} \psi_d^2 |\mathbf{p}_d|^2 \sin\vartheta d\vartheta d\varphi \quad , \quad (4)$$

where the integration limits are given by the intervals of the azimuthal angle and the polar angle covered by the incident light. The above expression is solved for ψ_d :

$$\psi_d = \frac{\sqrt{2P}}{f \sqrt{\epsilon_0 c \Delta\Omega_d}} \quad , \quad (5)$$

where $\Delta\Omega_d$ is the solid angle weighted by the dipole radiation pattern:

$$\Delta\Omega_\pi = \left[\frac{\cos^3\vartheta}{3} - \cos\vartheta \right]_{\vartheta_1}^{\vartheta_2} \cdot (\varphi_2 - \varphi_1) \quad (6)$$

for a linear dipole and

$$\Delta\Omega_{\sigma_\pm} = \frac{1}{2} \left[-\frac{\cos^3\vartheta}{3} - \cos\vartheta \right]_{\vartheta_1}^{\vartheta_2} \cdot (\varphi_2 - \varphi_1) \quad (7)$$

for a circular dipole.

Inserting the corresponding polarization vector \mathbf{p}_d and the factor ψ_d into Eq. 1 and performing the integration for a linear dipole as well as for circular dipoles, one obtains a general relation for the field component parallel to the virtual dipole:

$$\mathbf{E}_d(0) = -i \frac{\sqrt{2P}}{\lambda \sqrt{\epsilon_0 c}} \cdot \sqrt{\Delta\Omega_d} \quad . \quad (8)$$

This emphasizes that in order to maximize the focal field component parallel to a given virtual dipole one has to (i) put as much of the incident power as possible into the corresponding dipole mode and (ii) maximize the solid angle covered by the incident radiation. It should be pointed out that the resulting field strength does not depend on the dipole type.

We note that for full solid angle illumination the field given by Eq. 8 delivers exactly the maximum possible electric energy density given by Bassett [12]. Furthermore, Eq. 8 constitutes the generalization of Eqs. 8 and 10 of Ref. [11], where the case of a linear dipole oriented along the optical axis of an objective obeying the sine condition is treated. However, the connection to dipole radiation was not established there.

III. OPTIMUM IRRADIANCE DISTRIBUTIONS

Next, we want to derive the ideal radiation patterns incident onto the focusing device which are transformed into a dipole

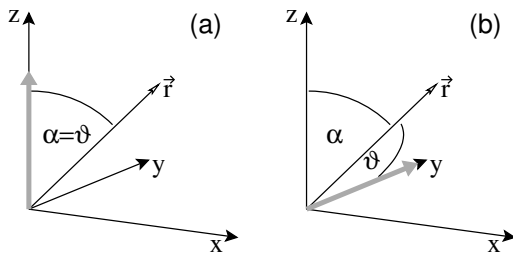


FIG. 1: Relation of the angles α and ϑ to the Cartesian coordinates: (a) dipole/quantization axis (gray arrow) parallel to the optical axis; (b) dipole/quantization axis perpendicular to the optical axis.

wave that moves towards the focus. For all devices treated here, we assume that they operate perfectly, i.e., the wave incident onto the focus is assumed to have a uniform phase after reflection/refraction off the focusing device (see also Ref. [10]). For example, a parabolic mirror might exhibit (small) deviations from the perfect parabolic shape. Furthermore, the phase shift upon reflection is different for different angles of incidence. We presuppose that such effects are compensated for by, e.g., appropriate correcting elements. The production of such elements and the measurement of imperfections might turn out to be a challenging but feasible experimental task [25].

The method is simply to start with a dipole wave which virtually emerges from the focus and trace it back through the optical element under consideration. We have chosen to formulate the ideal radiation patterns in terms of irradiances instead of field vectors, since the former quantity is the one usually measured in an experiment. Furthermore, in the derivation of the apodization factors carried out below, energy conservation considerations require the use of irradiances and radiant intensities anyway. The ideal vectors fields can be constructed from the irradiance patterns and the polarization patterns derived in the next section.

The derivation of the intensity patterns is pursued in the same way as it was done in Ref. [6] for a parabolic mirror and a linear dipole oriented parallel to the optical axis of the mirror. We designate by α the angle that is enclosed by the optical axis of the focusing element and the propagation direction of a single ray which hits the optical element at a distance r from the optical axis. Here, we chose the optical axis to coincide with the z -axis (cf. Fig. 1). Energy conservation demands that [6]

$$\Upsilon(\alpha) \sin \alpha d\alpha = I(r)r dr \quad , \quad (9)$$

which delivers

$$I(r) = \Upsilon(\alpha) \cdot A(r, \alpha) \quad , \quad (10)$$

with $A(r, \alpha) = \frac{\sin \alpha(r)}{r} \frac{d\alpha(r)}{dr}$ being an apodization factor. $\Upsilon(\alpha)$ is the radiant intensity, i.e., the light power emitted into an infinitesimal solid angle. $I(r)$ is the irradiance of the incident plane wave, i.e., the light power incident onto an infinitesimal surface area.

In what follows, we express the apodization factor as a function of the Cartesian coordinates x, y in the plane per-

pendicular to the optical axis: $A(x, y) = A(r(x, y))$ with $r = \sqrt{x^2 + y^2}$. In the case of a parabolic mirror, α is given through the relation [6]

$$\tan \frac{\alpha}{2} = \frac{r}{2f} \quad , \quad (11)$$

which with the help of some algebra leads to

$$A_{PM}(x, y) = \frac{1}{f^2 \left(\frac{x^2}{4f^2} + \frac{y^2}{4f^2} + 1 \right)^2} \quad . \quad (12)$$

For an aplanatic lens that fulfills the sine condition, i.e., a lens where the refracted rays of same phase seem to emerge from a spherical surface around the focus, one has

$$\sin \alpha = \frac{r}{f} \quad , \quad (13)$$

resulting in

$$A_{AL}(x, y) = \frac{1}{f^2 \sqrt{1 - \frac{x^2}{f^2} - \frac{y^2}{f^2}}} \quad . \quad (14)$$

As a third focusing element, we consider an ideal thin lens, i.e., a lens for which the refracted rays seem to emerge from a plane perpendicular to the optical axis. A practical realization of such a thin lens would be an idealized diffractive optical lens. One has

$$\tan \alpha = \frac{r}{f} \quad , \quad (15)$$

which delivers

$$A_{TL}(x, y) = \frac{1}{f^2 \left(\frac{x^2}{f^2} + \frac{y^2}{f^2} + 1 \right)^{3/2}} \quad . \quad (16)$$

Next, for every point (x, y) in the plane perpendicular to the optical axis we determine ϑ . The radiant intensity along this direction is given by the angular dipole radiation pattern $D(\vartheta)$:

$$\Upsilon(\vartheta) = D_0 \cdot D(\vartheta) \quad , \quad (17)$$

where D_0 is a proportionality constant. Finally, $\Upsilon(\vartheta)$ is also expressed in terms of x, y and multiplied with the apodization factor $A(x, y)$ yielding the irradiance $I(x, y)$.

If the dipole is oriented parallel to the optical axis, α coincides with ϑ (see Fig. 1a). Hence, the ideal irradiation is rotationally symmetric with respect to the optical axis and the angular dipole emission patterns given above can be written as $D_{\pi, \sigma_{\pm}}(\vartheta) = D_{\pi, \sigma_{\pm}}(\alpha)$. Using Eqs. 11, 13 and 15, respectively, and applying several trigonometric relations one obtains the ideal irradiance distributions. They are summarized in Tab. I and plotted in Fig. 2. We have also introduced normalized coordinates $X = x/f, Y = y/f, R = r/f$. All remaining dimensional quantities have been lumped into a proportionality constant I_0 .

TABLE I: Optimum irradiance distributions $I(R)$ for the creation of radiation patterns of dipoles oriented parallel to the optical axis of the focusing device. $R = r/f$ is the radial coordinate transverse to the optical axis given in units of the focal length. The proportionality constant I_0 contains all dimensional quantities.

	parabolic mirror	aplanatic lens	ideal thin lens
linear dipole	$I_0 \cdot \frac{R^2}{(\frac{R^2}{4} + 1)^4}$	$I_0 \cdot \frac{R^2}{\sqrt{1-R^2}}$	$I_0 \cdot \frac{R^2}{(R^2 + 1)^{\frac{5}{2}}}$
circular dipole	$I_0 \cdot \frac{\frac{R^4}{16} + 1}{(\frac{R^2}{4} + 1)^4}$	$I_0 \cdot \frac{1 - \frac{R^2}{2}}{\sqrt{1-R^2}}$	$I_0 \cdot \frac{1 + \frac{R^2}{2}}{(R^2 + 1)^{\frac{5}{2}}}$

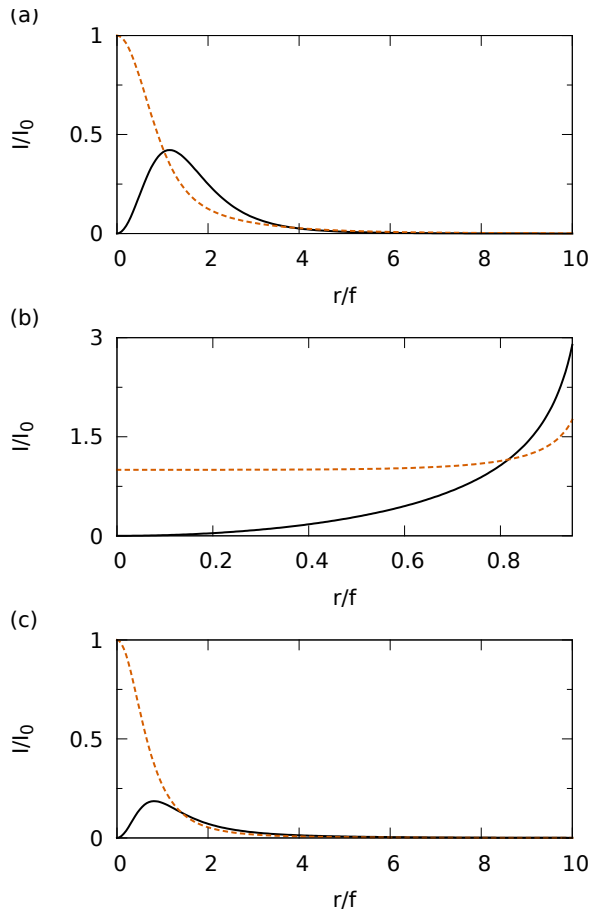


FIG. 2: Ideal irradiance distributions for dipoles oriented parallel to the optical axis of the focusing device: (a) parabolic mirror, (b) aplanatic lens fulfilling the sine condition, (c) ideal thin lens. Solid (dashed) lines denote the irradiance for a linear (circular) dipole radiation pattern.

The formula obtained here for the irradiance in the case of an aplanatic lens fulfilling the sine condition and a linear dipole corresponds exactly to the square of the formula for the electric field amplitude in the entrance pupil of the lens as it was found by means of an optimization method in Ref. [11].

Next, we turn to the case of the virtual dipole being oriented perpendicular to the optical axis of the focusing ele-

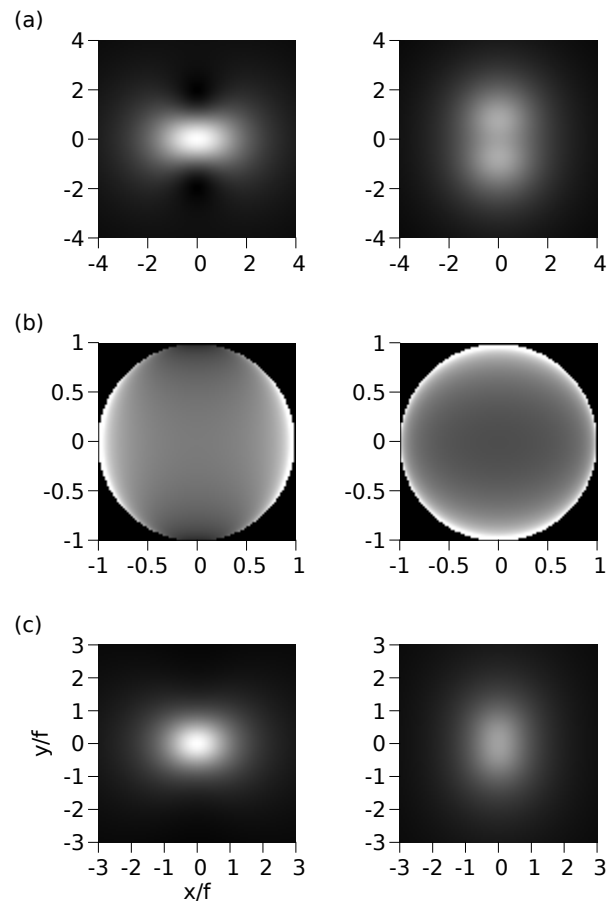


FIG. 3: Ideal irradiance distributions for dipoles oriented orthogonal to the optical axis of the focusing device: (a) parabolic mirror, (b) lens fulfilling the sine condition, (c) ideal thin lens. Left panel: linear dipole; right panel: circular dipole. The gray levels designate values of I/I_0 ranging from 0 (black) to 1 (white) in (a,c) and from 0 (black) to 3 (white) in (b).

ment. Without loss of generality we choose the virtual dipole axis (the direction $\vartheta=0$) to coincide with the y -axis (see Fig. 1b). An immediate consequence of the dipole axis being orthogonal to the optical axis is that the ideal intensity distributions have no longer rotational symmetry with respect to the optical axis. Furthermore, the angles α and ϑ do not coincide any more. Thus, the relations given by Eqs. 11, 13 and 15 can-

not be used to express the angular emission patterns $D_{\pi, \sigma_{\pm}}(\vartheta)$ in terms of the transverse coordinates. Instead one has to use in the case of the parabolic mirror the relations

$$\cos \vartheta = \frac{y}{\sqrt{x^2 + y^2 + z^2}}, \quad z = f - \frac{x^2 + y^2}{4f}. \quad (18)$$

This is valid if the focus of the parabolic mirror is located in the origin of the coordinate system. For a lens obeying the sine condition the relation between ϑ and x, y reads

$$\cos \vartheta = \frac{y}{f}, \quad (19)$$

and for the ideal thin lens one has

$$\tan \vartheta = \frac{\sqrt{x^2 + f^2}}{y}. \quad (20)$$

Again, the focus is located in the origin of the coordinate system. Using some trigonometric relations and multiplication with the corresponding apodization factors leads to the ideal irradiance distributions given in Tab. II and displayed in Fig. 3.

IV. OPTIMUM STATES OF POLARIZATION

Again, we begin the discussion for a virtual dipole parallel to the optical axis. For a linear dipole, the polarization pattern can be obtained immediately from the fact that the polarization vector of a linear dipole is oriented along \mathbf{e}_{ϑ} in the far field. This results in the well known radial polarization pattern [6, 14, 15] and, of course, coincides with the result found recently by optimization [11]. The polarization pattern is the same for all of the devices discussed here.

The situation is slightly more complex in the case of a circular dipole. The polarization vector for a certain ϑ is given by $\mathbf{p}_{\sigma_{\pm}}$ in Eq. 3. It can be rewritten as a unit vector

$$\hat{\mathbf{p}}_{\sigma_{\pm}} = \frac{\cos \vartheta \mathbf{e}_{\vartheta} \pm i \mathbf{e}_{\varphi}}{\sqrt{1 + \cos^2 \vartheta}} \quad (21)$$

by factoring out $(\cos \vartheta \pm i \sin \vartheta)/\sqrt{2}$ from $\mathbf{p}_{\sigma_{\pm}}$ for σ_{\pm} light, respectively. Using the relations given in Ref. [26] the normalized Stokes parameter S_3/S_0 describing the degree of circular polarization is then readily determined to be

$$\frac{S_{3\sigma_{\pm}}}{S_{0\sigma_{\pm}}} = \frac{\pm 2 \cos \vartheta}{1 + \cos^2 \vartheta}, \quad (22)$$

where S_0 corresponds to the total intensity and S_3 to the intensity that would be measured after passing the beam through a circular polarizer. With $S_3/S_0 = \sin(2\chi)$ giving the so called ellipticity angle [27], the ellipticity as a function of ϑ is

$$\chi_{\sigma_{\pm}} = \frac{\arcsin\left(\frac{\pm 2 \cos \vartheta}{1 + \cos^2 \vartheta}\right)}{2}, \quad (23)$$

where $\chi_{\sigma_{\pm}} = \pm\pi/4$ corresponds to circular states of polarization. This shows that the ideal polarization pattern for circular

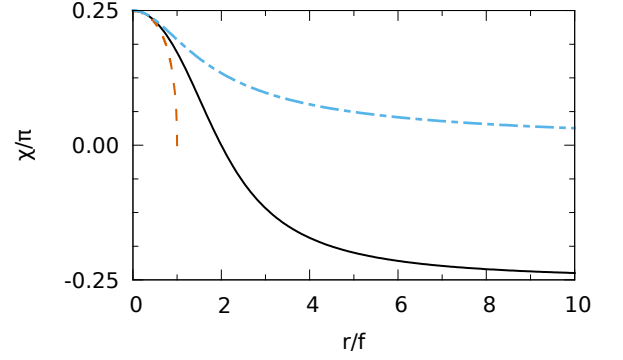


FIG. 4: Ellipticity of the ideal states of polarization for a circular dipole (σ_+ , a sign change gives the values for σ_-) oriented parallel to the optical axis of the focusing device. Solid line: parabolic mirror; dashed line: aplanatic lens; dash-dotted line: ideal thin lens.

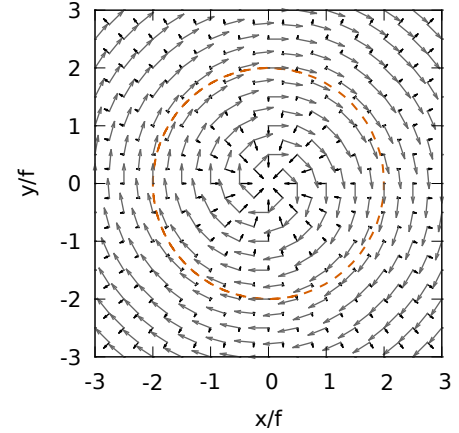


FIG. 5: State of polarization of the ideal radiation pattern for the case of a parabolic mirror and a circular dipole (σ_+) with the dipole axis oriented parallel to the optical axis of the mirror. The vectors in gray color denote the linearly polarized components with $\pi/2$ phase shift. The dashed line denotes the boundary $\text{NA}=1$.

dipoles exhibits a varying ellipticity as a function of the radial distance to the optical axis.

Using Eqs. 11, 13 and 15 to express ϑ through r , one obtains the ideal state of polarization for the different focusing devices. The results are displayed in Fig. 4. Note that in the case of the parabolic mirror there is a sign change of the ellipticity at the radius $r = 2f$, which corresponds to a half opening angle of the parabolic mirror of 90° . This result explains the finding of Ref. [10](Fig. 2) that an increase of the half focusing angle beyond 90° does not lead to a substantial decrease of focus size for an incident wave that has a circular state of polarization of same helicity over the whole beam cross section.

The long axis of the polarization ellipse for each ϑ is given by $\pm \mathbf{e}_{\varphi}$, i.e., the long axis of the polarization ellipse is oriented azimuthally. In other words, the state of polarization that creates the radiation pattern of a circular dipole parallel

TABLE II: Optimum irradiance distributions $I(X, Y)$ for the creation of radiation patterns of dipoles oriented orthogonal to the optical axis of the focusing device. $X = x/f$ and $Y = y/f$ are the coordinates transverse to the optical axis given in units of the focal length. The proportionality constant I_0 contains all dimensional quantities.

	parabolic mirror	aplanatic lens	ideal thins lens
linear dipole	$I_0 \cdot \frac{1 - \frac{Y^2}{X^2 + Y^2 + (X^2/4 + Y^2/4 - 1)^2}}{(X^2/4 + Y^2/4 + 1)^2}$	$I_0 \cdot \frac{1 - Y^2}{\sqrt{1 - X^2 - Y^2}}$	$I_0 \cdot \frac{1 + X^2}{(X^2 + Y^2 + 1)^{5/2}}$
circular dipole	$I_0 \cdot \frac{1/2 + \frac{Y^2/2}{X^2 + Y^2 + (X^2/4 + Y^2/4 - 1)^2}}{(X^2/4 + Y^2/4 + 1)^2}$	$I_0 \cdot \frac{1/2 + Y^2/2}{\sqrt{1 - X^2 - Y^2}}$	$I_0 \cdot \frac{Y^2 + \frac{X^2 + 1}{2}}{(X^2 + Y^2 + 1)^{5/2}}$

to the optical axis is a mixture of circular and azimuthal polarization, with the relative amount of the two depending on ϑ (i.e., the radial position r in the entrance plane of the focusing device): The circularly polarized fraction scales with $2 \cos \vartheta$, whereas the polar fraction is proportional to $1 - \cos^2 \vartheta$. The last statement can be inferred as follows: At each angle ϑ , the intensity measured after a polarizer parallel to \mathbf{e}_φ is proportional to unity. The intensity measured after a polarizer oriented orthogonal to \mathbf{e}_φ , i.e., along \mathbf{e}_θ , is proportional to $\cos^2 \vartheta$. The difference of the two gives the first Stokes parameter [27], which in this case (locally) measures the amount of light that is linearly polarized along \mathbf{e}_φ . The polarization pattern is depicted exemplarily in Fig. 5 for a parabolic mirror.

If the dipole axis is orthogonal to the optical axis, the polarization pattern of the ideal wave creating a certain kind of dipole radiation acquires more complexity. We will describe the polarization patterns in an exemplary way for the parabolic mirror. The polarization patterns do not change qualitatively for the other two devices treated here.

The polarization pattern is obtained as follows: The state of polarization $\mathbf{p}_{\vartheta, \varphi}$ of the virtual dipole, formulated in terms of the spherical unit vectors $\mathbf{e}_{\vartheta, \varphi}$, is transformed into the Carte-

sian coordinate system: $\mathbf{p}_{\vartheta, \varphi} \rightarrow \hat{\mathbf{p}}_{x, y, z}$, where $\hat{\mathbf{p}}_{x, y, z}$ is a vector of length unity. Recall, that in the case at hand the direction $\vartheta = 0$ coincides with the positive y -axis. This is handled by interchanging the second with the third component of the unit vectors $\mathbf{e}_{\vartheta, \varphi}$ of the spherical coordinate system. Then, the ray for each emission direction is traced from the virtual dipole towards the surface of the parabolic mirror. The polarization vector of the ray after reflection at the mirror surface is calculated via the following equation:

$$\hat{\mathbf{p}} = 2(\hat{\mathbf{p}}_{x, y, z} \cdot \mathbf{N})\mathbf{N} - \hat{\mathbf{p}}_{x, y, z} \quad , \quad (24)$$

with the surface normal of the mirror given by

$$\mathbf{N} = \frac{1}{\sqrt{\frac{x^2 + y^2}{4f^2} + 1}} \begin{pmatrix} \frac{x}{2f} \\ \frac{y}{2f} \\ 1 \end{pmatrix} \quad . \quad (25)$$

Again, the focus is chosen to be at the origin of the coordinate system. Using Eqs. 2 and 3, one obtains the polarization patterns

$$\hat{\mathbf{p}}_\pi(X, Y) = \frac{1}{\sqrt{(X^2 + Y^2 + 4)^2 - 16Y^2}} \begin{pmatrix} 2XY \\ Y^2 - X^2 - 4 \end{pmatrix} \quad (26)$$

for a linear dipole and

$$\begin{aligned} \hat{\mathbf{p}}_{\sigma_\pm}(X, Y) = & \frac{Y}{\sqrt{(X^2 + Y^2 + 4)^2 - 16Y^2}} \begin{pmatrix} -\frac{XY}{4} \\ \frac{X^2 - Y^2}{4} + 1 \end{pmatrix} \\ & \pm i \frac{\frac{X^2 + Y^2}{4} + 1}{\sqrt{\left[X^2 + \left(1 - \frac{X^2 + Y^2}{4}\right)^2\right] \left[Y^2 + \left(1 + \frac{X^2 + Y^2}{4}\right)^2\right]}} \begin{pmatrix} \frac{X^2 - Y^2}{4} + 1 \\ \frac{XY}{2} \end{pmatrix} \end{aligned} \quad (27)$$

for the circular dipoles. The two polarization patterns are illustrated in Fig. 6. Up to the boundary given by $\sqrt{X^2 + Y^2} = 2$ (or numerical aperture NA=1), the polarization pattern is

qualitatively similar for the other focusing devices treated here. However, one has to keep in mind that the relations between ϑ , φ and the Cartesian coordinates in the entrance

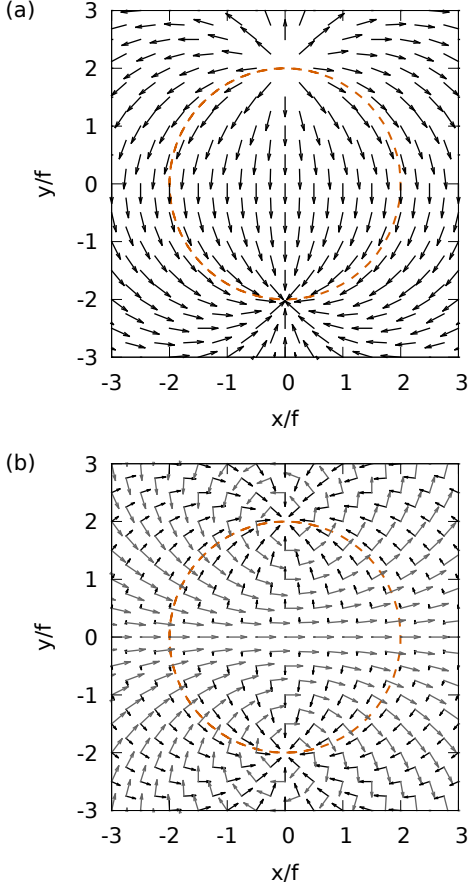


FIG. 6: State of polarization of the ideal radiation patterns for the case of a parabolic mirror and the dipole axis oriented orthogonal to the optical axis of the mirror: (a) linear dipole, (b) circular dipole (σ_+). In (b) the vectors in gray color denote the linearly polarized components with $\pi/2$ phase shift. The dashed line denotes the boundary $\text{NA}=1$.

plane of the devices are different. Thus, the pattern displayed inside the circle marking $\text{NA}=1$ in Fig. 6 will be distorted or stretched/compressed to some amount, respectively.

V. OVERLAP OF PRACTICAL DISTRIBUTIONS WITH THE IDEAL ONES

Some of the radiation patterns derived above – namely in the case of the dipole axis parallel to the optical axis – exhibit obvious similarities with radiation modes which are commonly used in experiments. In the case of a parabolic mirror and the ideal thin lens, the irradiance distributions for a linear virtual dipole look close to the well known doughnut modes. In the case of circular virtual dipoles there is a strong similarity with fundamental Gaussian distributions.

In order to estimate and quantify the strength of the similarities, we will calculate the overlap of these modes with the ideal radiation distributions. The discussion is limited to the case that the dipoles are oriented parallel to the optical axis.

We begin with defining the overlap on the focal sphere as

$$\eta = 2\pi \int \mathbf{E}_i^*(\vartheta) \cdot \mathbf{E}_f(\vartheta) \sin \vartheta d\vartheta \quad , \quad (28)$$

where \mathbf{E}_i is the ideal field and \mathbf{E}_f the incident field. The integration is performed over the polar angle covered by the focusing optics. For the sake of simplicity, we make the approximation that the polarization vector of the incident field is everywhere parallel to the polarization vector of the ideal distribution. We can then write the overlap in terms of the field moduli or the radiant intensities $\Upsilon(\vartheta)$, respectively, as

$$\eta = \frac{4\pi}{\epsilon_0 c f^2} \int \sqrt{\Upsilon_i(\vartheta)} \sqrt{\Upsilon_f(\vartheta)} \sin \vartheta d\vartheta \quad . \quad (29)$$

Identifying ϑ with α in Eq. 9 and taking the square root of Eq. 9 we have

$$\eta = \frac{4\pi}{\epsilon_0 c f^2} \int \sqrt{I_i(r)} \sqrt{I_f(r)} r dr \quad . \quad (30)$$

This is the (expected) result that the overlap on the focal sphere is the same as the overlap in the entrance plane of the focusing optics. Finally, we normalize the overlap to the power contained in the ideal and the incident field and arrive at

$$\eta_N = \frac{\int \sqrt{I_i(r)} \sqrt{I_f(r)} r dr}{\sqrt{\int I_i(r) r dr} \cdot \sqrt{\int I_f(r) r dr}} \quad . \quad (31)$$

Next, the normalized overlap is related to the field amplitude in the focus. We expand the field on the focal sphere in terms of the electric dipole components as

$$\mathbf{E}_f = \psi_\pi \mathbf{p}_\pi + \psi_{\sigma_+} \mathbf{p}_{\sigma_+} + \psi_{\sigma_-} \mathbf{p}_{\sigma_-} + \dots \quad . \quad (32)$$

Magnetic dipole terms and higher order multipole terms are neglected since they do not contribute to the electric field in the focus anyway [12]. Taking the integral $\int d\varphi d\vartheta \sin \vartheta \mathbf{p}_d^*$ on both sides, where $d = \pi, \sigma_\pm$ and \mathbf{p}_d is given by Eqs. 2 and 3, one finds

$$2\pi \int \mathbf{p}_d^* \cdot \mathbf{E}_f \sin \vartheta d\vartheta = \psi_d \cdot \Delta\Omega_d \quad , \quad (33)$$

since the different kinds of dipole fields are orthogonal for full azimuthal angle integration. Dividing both sides by $(2\pi \int |\mathbf{E}_f|^2 \sin \vartheta d\vartheta \cdot 2\pi \int |\mathbf{p}_d|^2 \sin \vartheta d\vartheta)^{1/2}$ gives

$$\eta_{N,d} = \psi_d \times \frac{\sqrt{\Delta\Omega_d}}{\sqrt{2\pi \int |\mathbf{E}_f|^2 \sin \vartheta d\vartheta}} \quad (34)$$

with $\eta_{N,d}$ the normalized overlap on the focal sphere calculated for a specific ideal dipole radiation of kind d . For any given input power, the field in the focus parallel to a certain virtual dipole is maximized when the complete incident power is contained in the corresponding dipole wave, i.e., ψ_d is maximized: $\mathbf{E}_f = \psi_{d,\max} \mathbf{p}_d$. This means that

$$2\pi \int |\mathbf{E}_f|^2 \sin \vartheta d\vartheta = \psi_{d,\max}^2 \cdot \Delta\Omega_d \quad . \quad (35)$$

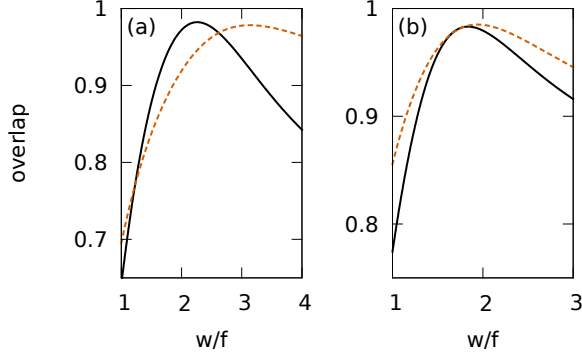


FIG. 7: Normalized overlap of the ideal field distributions with common radiation modes as a function of the modes beam radius w in units of the focal length f . The virtual dipoles are oriented parallel to the optical axis. (a) Parabolic mirror with a half opening angle of 134° . (b) Ideal thin lens with a numerical aperture of 0.95. Solid lines: Overlap of the ideal field for linear dipoles with a radially polarized doughnut mode. Dashed lines: Overlap of the ideal field for circular dipoles with a fundamental Gaussian mode that has an ideal state of polarization.

Inserting this into Eq. 34 finally reveals that

$$\eta_{N,d} = \frac{\psi_d}{\psi_{d,\max}} \quad (36)$$

Thus, the fraction of the achievable field modulus in the focus with relation to the maximum possible one is directly proportional to the overlap $\eta_{N,d}$ on the focal sphere or the overlap in the entrance plane of the focusing optics, respectively. In other words, if the incident wave is not a pure dipole wave, the right hand side of Eq. 8 has to be multiplied by a factor $\eta_{N,d}$:

$$\mathbf{E}_d(0) = -i \frac{\sqrt{2P}}{\lambda\sqrt{\epsilon_0 c}} \cdot \sqrt{\Delta\Omega_d} \cdot \eta_{N,d} \quad (37)$$

Figure 7 shows some examples for illustration. In the case of a parabolic mirror with a half opening angle of 134° as it is used in the experiment described in Refs. [6, 7], a radially polarized doughnut mode ($\sqrt{I(r)} \sim r \cdot e^{-r^2/w^2}$, w is the beam radius) best matches the field distribution for a linear dipole at a beam radius of $w/f = 2.26$. There, the overlap is $\eta_{N,\pi} = 0.982$. The half opening angle of 134° corresponds to $\Delta\Omega_\pi = 0.94 \times 8\pi/3$. Thus, the field amplitude parallel to the virtual linear dipole would be 0.95 times the one obtained with the ideal radiation pattern and a parabolic mirror of infinite dimensions. This has been confirmed in simulations. In the case of a circular dipole, the maximum overlap of $\eta_{N,\sigma_\pm} = 0.978$ is achieved for a Gaussian fundamental mode ($\sqrt{I(r)} \sim e^{-r^2/w^2}$) with a beam waist of $w/f = 3.14$. With $\Delta\Omega_{\sigma_\pm} = 0.80 \times 8\pi/3$ one achieves a field amplitude parallel to the virtual circular dipole of 0.87 times the maximum possible one.

For an ideal thin lens (Fig. 7b) with NA=0.95 the optimum overlap of $\eta_{N,\pi} = 0.983$ is reached at $w/f = 1.84$ (linear

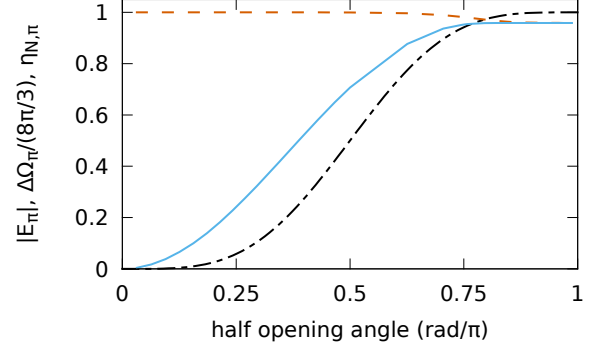


FIG. 8: Solid angle $\Delta\Omega_\pi/(8\pi/3)$ (dash-dotted line), maximum possible overlap $\eta_{N,\pi}$ with a linear dipole wave (dashed line) and field amplitude $|E_\pi|$ in the focus in units of the maximum possible one (solid line) as the function of the half opening angle of a parabolic mirror. For further explanations see text.

dipole) and the maximum value of $\eta_{N,\sigma_\pm} = 0.985$ reached at $w/f = 1.94$ (circular dipole). With $\Delta\Omega_\pi = 0.27 \times 8\pi/3$ and $\Delta\Omega_{\sigma_\pm} = 0.38 \times 8\pi/3$ one achieves 0.51 and 0.61 times the field amplitudes of the maximum possible ones, respectively.

Please note that for the parabolic mirror as well as for the ideal thin lens the optimum beam waist of the doughnut is such that the maximum of the irradiance distribution is located at a somewhat larger radial position than the maximum of the radiation patterns of a linear dipole that are displayed in Fig. 2(a,c). Furthermore, the values for the circular dipoles given above have to be considered as upper limits in the sense that the ideal state of polarization for a circular dipole is difficult to obtain in practice.

If the solid angle covered by the focusing optics is increased, the maximum achievable overlap of the 'simple' modes with the ideal distributions decreases. However, this is overcompensated for by an increase in solid angle, i.e., the field in the focus parallel to a specific virtual dipole is maximized by maximizing the solid angle, as long as the simple mode is polarized parallel to the ideal polarization across the whole beam cross section. This is illustrated in Fig. 8 for a linear dipole and a parabolic mirror (in the case of a circular dipole and/or a thin lens the results are qualitatively similar). For each (half) opening angle of the mirror the maximum overlap is obtained from a curve like the one in Fig. 7(a). The resulting field is then obtained from Eq. 37 by inserting the overlap value and the corresponding square root of the covered solid angle into this equation.

From the asymptotic behavior of the plot for the field amplitude in Fig. 8 one can extract the maximum field amplitude one could achieve with a doughnut mode of suitable polarization by focusing the mode with a parabolic mirror. Likewise, one obtains the same values for circular dipoles (i.e., overlapping with a Gaussian mode of proper polarization) and/or an ideal thin lens. The values are listed in Tab. III.

One could calculate the overlaps also in the case of a lens obeying the sine condition. However, due to the divergence of the ideal irradiance values towards the boundary of the lens

TABLE III: Maximum electric field amplitudes achievable by use of a radially polarized doughnut mode and a fundamental Gaussian mode with the state of polarization matching a circular dipole. The values are given relative to the ones obtainable with the ideal irradiance distributions of Fig. 2(a,c). The virtual dipoles are oriented parallel to the optical axis.

	doughnut mode	fundamental Gaussian
parabolic mirror	0.958	0.919
ideal thin lens	0.575	0.628

aperture the calculation of the overlap with the simple modes discussed above does not appear to be meaningful. Similar arguments apply when the virtual dipole is oriented orthogonal to the optical axis. Since the ideal irradiance patterns have no rotational symmetry, the overlaps will always be smaller than their counterparts for the dipole axis being parallel to the optical axis.

VI. CONCLUDING REMARKS

We have derived the ideal radiation patterns with which one achieves the maximum possible field strengths for several fo-

cusing devices. Besides using these radiation patterns, it is of utmost importance to maximize the covered solid angle, as it is shown by Eqs. 8 and 37. Thus, the maximum possible electric field strength is achieved by covering the full solid angle. Also, the maximum possible effect in the interaction of light with single atoms will also only be found for full solid angle coverage, since scattering as well as absorption of photons is proportional to the square of the electric field amplitude at the location of the atom [26]. This finding is in contrast to the statements made in other publications, where it was claimed that the power scattered by a single atom is already maximized for half solid angle illumination [4, 5]. According with the papers of Van Enk and Kimble [16, 28], we want to state once more that for optimum interaction of light with single atoms one has to shape the radiation incident onto the atom to resemble an electric dipole wave.

-
- [1] A. N. Vamivakas, M. Atatüre, J. Dreiser, S. T. Yilmaz, A. Badolato, A. K. Swan, B. B. Goldberg, A. Imamoglu, and M. S. Ünlü, *Nano Letters* **7**, 2892 (2007).
 - [2] G. Wrigge, I. Gerhardt, J. Hwang, G. Zumofen, and V. Sandoghdar, *Nature Physics* **4**, 60 (2008).
 - [3] M. K. Tey, Z. Chen, S. A. Aljunid, B. Chng, F. Huber, G. Maslennikov, and C. Kurtsiefer, *Nature Physics* (2008).
 - [4] M. K. Tey, S. A. Aljunid, F. Huber, B. Chng, Z. Chen, G. Maslennikov, and C. Kurtsiefer, arXiv:0804.4861 (2008).
 - [5] G. Zumofen, N. M. Mojarad, V. Sandoghdar, and M. Agio, *Physical Review Letters* **101**, 180404 (2008).
 - [6] N. Lindlein, R. Maiwald, H. Konermann, M. Sondermann, U. Peschel, and G. Leuchs, *Laser Physics* **17**, 927 (2007).
 - [7] M. Sondermann, R. Maiwald, H. Konermann, N. Lindlein, U. Peschel, and G. Leuchs, *Appl. Phys. B* **89**, 489 (2007).
 - [8] D. Pinotsi and A. Imamoglu, *Phys. Rev. Lett.* **100**, 093603 (2008).
 - [9] J. Stadler, C. Stanciu, C. Stupperich, and A. J. Meixner, *Opt. Lett.* **33**, 681 (2008).
 - [10] N. Bokor and N. Davidson, *Opt. Commun.* **281**, 5499 (2008).
 - [11] H. P. Urbach and S. F. Pereira, *Physical Review Letters* **100**, 123904 (2008).
 - [12] I. M. Basset, *Journal of Modern Optics* **33**, 279 (1986).
 - [13] C. J. R. Sheppard and P. Török, *Optik* **104**, 175 (1997).
 - [14] S. Quabis, R. Dorn, M. Eberler, O. Glöckl, and G. Leuchs, *Opt. Comm.* **179**, 1 (2000).
 - [15] N. Bokor and N. Davidson, *Opt. Lett.* **29**, 1968 (2004).
 - [16] S. J. van Enk, *Phys. Rev. A* **69**, 043813 (2004).
 - [17] G. Lerosey, J. de Rosny, A. Tourin, A. Derode, G. Montaldo, and M. Fink, *Phys. Rev. Lett.* **92**, 193904 (2004).
 - [18] J. de Rosny and M. Fink, *Phys. Rev. Lett.* **89**, 124301 (2002).
 - [19] J. J. Stamnes and V. Dhayalan, *Pure Appl. Opt.* **5**, 195 (1996).
 - [20] C. J. R. Sheppard and P. Török, *J. Mod. Opt.* **44**, 803 (1997).
 - [21] V. Dhayalan and J. J. Stamnes, *Pure Appl. Opt.* **6**, 347 (1997).
 - [22] J. D. Jackson, *Classical Electrodynamics* (Wiley, New York, 1999), 3rd ed.
 - [23] M. Lieb and A. Meixner, *Opt. Express* **8**, 458 (2001).
 - [24] R. K. Wangsness, *Electromagnetic fields* (Wiley, 1986), 2nd ed.
 - [25] G. Leuchs, K. Mantel, A. Berger, H. Konermann, M. Sondermann, U. Peschel, N. Lindlein, and J. Schwider, *Applied Optics* **47**, 5570 (2008).
 - [26] L. Mandel and E. Wolf, *Optical Coherence and Quantum Optics* (Cambridge University Press, Cambridge, New York, 1995), ISBN 0 521 41711 2.
 - [27] E. Hecht, *Optics* (Addison-Wesley Publishing Company, 1987).
 - [28] S. J. van Enk and H. J. Kimble, *Phys. Rev. A* **63**, 023809 (2001).